Fission from Fe and Nb reactions with heavy targets at 50–100 MeV/nucleon

M. Begemann-Blaich,* Th. Blaich,† M. M. Fowler, and J. B. Wilhelmy
Los Alamos National Laboratory, Los Alamos, New Mexico 87545

H. C. Britt, D. J. Fields, L. F. Hansen, R. G. Lanier, D. J. Massoletti, M. N. Namboodiri, B. A. Remington, T. C. Sangster, G. L. Struble, and M. L. Webb‡
Lawrence Livermore National Laboratory, Livermore, California 94550

Y. D. Chan, A. Dacal,§ A. Harmon,** J. Pouliot,†† and R. G. Stokstad
Lawrence Berkeley Laboratory, Berkeley, California 94720

S. Kaufman and F. Videbaek‡‡
Argonne National Laboratory, Argonne, Illinois 60439

Z. Fraenkel
Weizmann Institute of Science, 76100 Rehovot, Israel
(Received 19 June 1991)

Cross sections, parallel and perpendicular momentum transfers, charge loss, and velocity systematics are presented for fission following reactions of Fe and Nb projectiles at 50–100 MeV/nucleon on targets of Ta, Au, and Th. Data are compared to simple models for peripheral heavy ion collisions.

PACS number(s): 25.70.Jj, 25.70.−z, 25.85.Ca

I. INTRODUCTION

The fission of a compound nucleus or target residue formed in a heavy ion collision provides a useful probe for investigating reaction dynamics. Fission is a well-defined collective mode which occurs toward the end of the reaction and the distinctive fragment Coulomb energy systematics are easily recognized. Measurement of the correlated momenta (or the folding angle) of the two fragments gives an estimate of the parallel and perpendicular momentum imparted to the fissioning source. The sum of the masses or charges of the fragments gives an estimate of the mass of the source. In turn, the mass loss and parallel momentum transfer can be used to estimate the initial excitation energy. For residue sources in the mass range 150 to 200, the probability of fission decay is a sensitive function of both the initial excitation energy and angular momentum.

Previous experiments on heavy ion induced fission at bombarding energies above 10 MeV/nucleon have shown that only part of the initial momentum and mass of the projectile is transferred to the fissioning source. At energies of 50–100 MeV/nucleon, the parallel momentum transfer per projectile nucleon decreases with both increasing mass and momentum of the projectile (see Ref. [1] for a review). This result is taken as evidence for the increasingly peripheral nature of the collisions feeding the fission channel. However, until recently very little data have been available in this higher energy regime for projectiles with masses greater than about 20.

In this paper we present data from a series of experiments at the Lawrence Berkeley Laboratory (LBL) Bevalac designed specifically for a systematic investigation of fission from intermediate energy heavy ion collisions with heavy projectiles. Results are presented for the reactions Nb+Au, and Fe+Ta, Au, Th at energies of 50, 75, and 100 MeV/nucleon. These systems span a wide range of projectile energies (2.8 to 9.3 GeV) and momenta (17 to 41 GeV/c). Furthermore, the three targets Ta, Au, and Th have vastly different fissilities (Z^2/A), so that fission is expected to sample different regions of excitation energy deposition and linear momentum transfer. For the 100 MeV/nucleon data presented in this paper a detailed comparison has been made to a model [2] combining a fast initial collision described by an intranuclear cascade model followed by a statistical decay of the target residue.

*Gesellschaft fuer Schwerionenforschung, KP3, Postfach 11 05 52, D-61 Darmstadt, Germany.
†Universitaet Mainz, Institut fuer Kernchemie, D-65 Mainz, Germany.
‡Dynamics Technology, 21311 Hawthorne Blvd., Torrance, California 90503.
§Instituto De Fisica, UNAM, Mexico, DF 01000, Mexico.
**Space Science Lab, NASA-Marshall Space Flight Center, Huntsville, AL 35812.
††Laboratoire de Physique Nucleaire, Universite Laval Ste Foy, Quebec, GIK7P4, Canada.
‡‡Brookhaven National Laboratory, Physics Dept., Bldg. 901A, Upton, NY 11973.

II. EXPERIMENTAL DETAILS

A. Apparatus

To measure the correlations among the extremely wide range of reaction products encountered at intermediate energies one needs a detector system with a large geometric coverage and a wide dynamic range in energy and particle type. Relatively slow moving highly ionizing fission fragments and target residues must be recorded simultaneously with low ionizing fast moving light particles. We have designed such a detector system for use at the LBL Bevalac low energy beam line. The detector system is called PAGODA and Fig. 1 shows a schematic of the installation at the Bevalac. A detailed description of the detector components and their responses is given in Ref. [3].

The apparatus consists of eight identical gas modules, six arrays of nine phoswich scintillator detectors behind the most forward six gas modules, and a 34 element phoswich projectile hodoscope. Each gas detector contains an 8 cm×16 cm position sensitive multiwire proportional counter (MWPC) followed by a low pressure proportional counter (PC), and a second MWPC with an active area of 16 cm×16 cm. These first three elements are operated in a common volume of isobutane at 2.5 Torr. Each MWPC provides submillimeter position resolution and a fast timing signal with a width of 400 ps. The difference between the two MWPC timing signals gives the time of flight (TOF) over the PC drift region (18 cm). Combined with a dE/dx measurement in the PC, this provides fragment charge and velocity identification over a large range of fragment energies. Since the anode and position efficiencies for light ions are reasonably high, timing information is available for essentially all fragments with $Z > 5$ and energy greater than about 200 keV/nucleon. The final element of each gas module is an ionization chamber (IC) located immediately behind the second MWPC. For fission fragments, Z identification is done exclusively with the TOF and PC information; the IC's and phoswich arrays are not used.

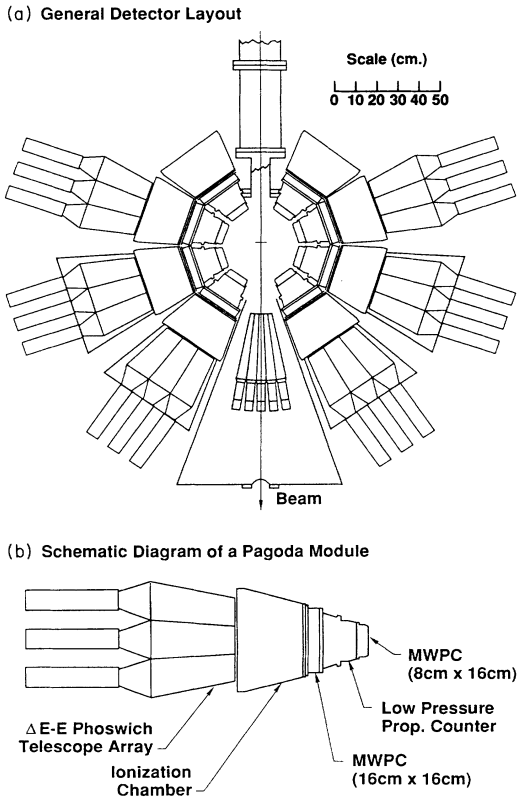

FIG. 1. (a) The PAGODA detector layout at the LBL Bevalac low energy beam line. The center lines of the modules are at 36°, 72°, 108°, and 144° on either side of the beam. The hodoscope is located in the wedge-shaped target chamber extension. (b) A detailed layout of a single PAGODA module.

The eight gas modules, covering approximately 13% of 4π, are arranged around the target in a cylindrical geometry between 24° and 158° in the beam plane and ±12° out of plane. In addition, the front MWPC's extend the coverage out of plane to ±25° (an additional 10% of 4π) but with significantly lower resolution for particle identification. The targets were self-supporting foils of Au, Ta, and Th with thicknesses of 1.34, 1.86, and 1.10 mg/cm^2, respectively. They were always positioned at 90° relative to the beam.

The thirty-four elements of the forward hodoscope are fast/slow plastic phoswich detectors. The array covers an angular range from 2° to 10° horizontally and from 2° to 14° vertically. Since the energy thresholds for particle identification are 9 MeV for protons and about 40 MeV/nucleon for Nb, this array is sensitive to the entire range of projectile fragments at the beam energies used in our experiments. The charge resolution for these modules is excellent. We observed unit Z resolution through the projectile charge for the Fe data; for the Nb data, the resolution was two Z units above $Z = 20$.

B. Calibration and particle identification

Excellent charge resolution for relatively slow particles could be obtained with the PC and TOF, whereas the IC was most useful in combination with the phoswich detectors for the identification of more energetic particles. To take advantage of the excellent PC resolution, we developed an identification scheme based on a series of calibration measurements made at the LANL Van de Graaff accelerator. A number of light and heavy ion beams (C, O, S, Br, and I) at energies between 0.5 and 5.0 MeV/nucleon were scattered from different target foils (Ti, Zr, Dy, and Au) into a detector module mounted at a polar angle of 30°. Using the scattered projectiles as well as the recoiling target nuclei, a nearly continuous range of TOFs and PC energy losses was measured. At these energies, the scattering is elastic so we were able to obtain energy and time-of-flight calibrations for both the scattered beam particles and the target recoils. After comparing the calibration data with various energy loss codes [4–6], we concluded that the codes do not adequately reproduce the measured energy loss and charge dependences. Therefore, we decided to construct an empirical charge and velocity calibration utilizing the extensive data set.

We combined the results of the calibration measurements and the easily identified charge bands for $Z < 10$ from our initial 100 MeV/nucleon Nb+Au experiment to generate two-dimensional grids of measured PC pulse height and TOF. One grid provided the particle charge with approximately unit Z resolution for intermediate mass fragments ($Z < 20$) and a resolution of three units for fission-mass fragments. The second grid provided the fragment velocity with a resolution of 0.05 cm/ns. Both grids were constructed independently of any dE/dx code. ^{252}Cf fragments were used to gain match and time align the experimental data from each module to the grid calibration. We tested this algorithm by analyzing fission fragments from a thin two-sided ^{252}Cf source and were able to reproduce accurately the known mean values for both the charge and the velocity distributions [7].

Using this scheme, Z identification is possible for particles with incident energies between 0.5 and 2.7 MeV/nucleon and $Z < 54$. There are virtually no fission fragments above this energy and charge cutoff; however, a significant number have energies less than 0.5 MeV/nucleon. For these slow fragments we distinguish only between heavier and lighter fragments because the PC resolution again becomes quite poor. However, we still have velocity information down to energies as low as 0.2 MeV/nucleon and in most cases a low velocity fragment has a higher velocity binary partner which allows the event to be identified as fission.

In order to increase the experimental solid angle and to maximize our acceptance for perpendicular momentum transfer we have defined two classes of fission data. In class I events, both fragments reach the second MWPC (out-of-plane angle $|\phi| < 12°$) and are fully identified using the PC-TOF grid. For class II events, one fragment is fully identified but the other is in the angular range $12° < |\phi| < 25°$ and is therefore only detected in the first MWPC. For the latter fragment we have only the position and a crude mass identification using the MWPC anode signal (which is roughly proportional to the PC). However, as the incompletely detected fragment is in coincidence with a fully identified fragment from the PC-TOF grid, we get the event start time from the fully identified fragment and can evaluate the velocity of the out-of-plane fragment from its single MWPC timing signal. Although the MWPC anode resolution is relatively poor for the out-of-plane fission mass fragments, the data can still be separated into several mass regions, allowing some kinematic evaluations beyond the calculation of the folding angle and the distribution of relative velocities.

C. Acceptance calculations

In order to estimate the total fission cross section and to transform the experimental observables into distributions that can be compared to theories or models, it is essential to understand the acceptance of the PAGODA array. Since our analysis shows that the data from both the Fe and Nb induced fission can be completely described by low energy fission systematics [8] (see Sec. III below), we used a parametrization of these systematics to create a simulation of our acceptance for fission events. The simulation assumed relative velocities from fission systematics [8], symmetric fission with a Z distribution having a FWHM of 26 units and a fragment angular distribution that was isotropic in the rest frame of the fissioning system. To avoid large errors due to energy loss and scattering both in the target and in the detectors, and to avoid any influence due to target absorption, we excluded fission fragments with polar angles between 72° and 108° relative to the beam axis both from the analysis and the simulation. We also excluded fragments that hit the outermost 5 mm of the x and y planes of all detectors and took into account the transmission of the MWPC's (94% each). Extensive testing showed that the detection probability was independent of the mass split. With reasonable assumptions concerning the relation between $P_\parallel$ and $P_\perp$ it was also found to be almost independent of the fragment angular distribution. Therefore, the acceptance depended primarily on the total linear momentum transferred to the fissioning nucleus and on the correlation between the parallel and perpendicular components of the linear momentum.

The calculated two-dimensional acceptance—relative to a 4π geometry—of the gas detectors for fission events as a function of $P_\parallel$ and $P_\perp$ of the fissioning system is shown in Fig. 2 for class I and class II events. The acceptance in $P_\perp$ is primarily related to the ϕ coverage. Events with small perpendicular momentum transfer have small relative azimuthal angles. So, having one of the fragments detected with an out-of-plane angle $< 12°$, the second one will most likely be found in the same angular region, i.e., the event will be in class I. Events with large perpendicular momentum transfer have on the average larger relative azimuthal angles and therefore a higher probability to be in class II. Thus, the probability for detecting class I events is largest for small values of the

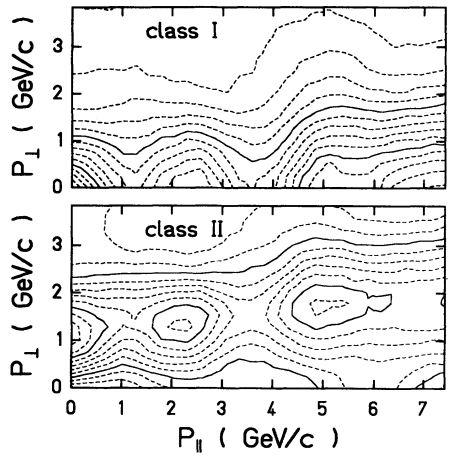

FIG. 2. Acceptance of the PAGODA array for class I (both fragments with $|\phi| < 12°$) and class II (one fragment with $12° < |\phi| < 25°$) events as a function of $P_\parallel$, $P_\perp$. The solid contours represent an acceptance of 2.5%, 5.0%, etc., while the dashed contours show steps of 0.5%. The closed solid contours in the bottom panel show 5% acceptance; in the upper panel, the 5% contour appears near the origin and for $P_\parallel > 4$ GeV/c and $P_\perp < 1$ GeV/c.

perpendicular momentum transfer, whereas the acceptance for class II events is very small for small $P_\perp$, reaches a maximum for $P_\perp \sim 1.5$ GeV/c, and then decreases with further increasing perpendicular momentum. The acceptance for parallel momentum transfer on the other hand is primarily sensitive to the θ coverage which is roughly the same for both classes of events, therefore leading to similar dependences on $P_\parallel$.

To deduce the acceptance for a given folding angle from the two-dimensional acceptance, the correlation between the parallel and perpendicular momentum components was taken from the data. As this correlation depends on the target/projectile combination (see Secs. III and IV), the resulting detection probabilities are slightly different for the different systems investigated, but the gross features do not change. In Fig. 3, the detection probability versus the folding angle for both classes of events is shown for the system Nb+Au at 100 MeV/nucleon. For zero parallel momentum transfer (folding angle $\theta_{FF}=180°$) the detection probability for class I fission events is given by the solid angle of the eight detectors. It should be noted that excluding the data between 72° and 108° reduces the solid angle of the gas modules to 6% of 4π. With increasing momentum transfer—i.e., decreasing folding angle—the acceptance shows modulations due to the gaps between the detectors.

D. Identification of fission events

We can easily identify the fission events using the correlation between the charges of the coincident fragments, shown in Fig. 4. As can be seen from the figure the events separate clearly into a fission and a nonfission region; moreover, there are no coincident events in the fission region between detectors located on the same side of the beam axis. On the other hand, it is clear that we cannot distinguish between the different processes which produce fragments in the fission mass region without using coincidence information. Both binary fission of the target residue and multiple fragment emission contribute to the inclusive distributions in the fission mass range. For further discussion see Ref. [9]. Similar results have been shown previously by Warwick *et al.* [10] and by Klotz-Engmann *et al.* [11].

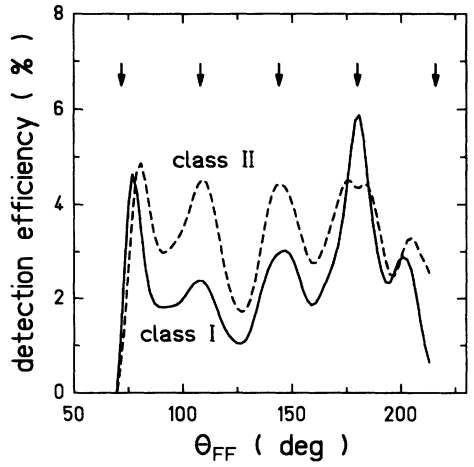

FIG. 3. Detection probability for fission events as a function of folding angle for both class I (solid) and class II (dashed) events. The arrows indicate the mean angles between different detector module combinations (72°, 108°, 144°, 180°, and 216°).

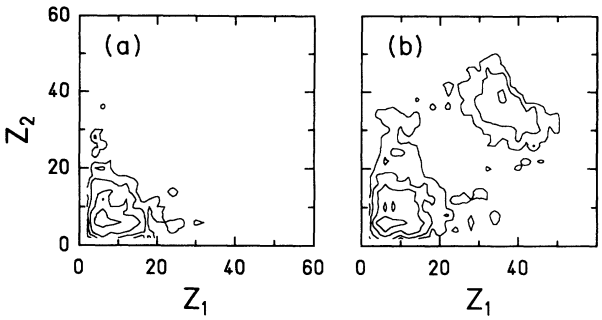

FIG. 4. (a) Contour plot of Z_1 vs Z_2 for coincidence events in which both fragments are detected on the same side of the beam. (b) The same plot except that Z_1 and Z_2 are now detected on opposite sides of the beam. The contours represent an increase in yield by factors of 2; the system is 100 MeV/nucleon Nb+Au.

Additional insight into this problem and, therefore, into the centrality of the reactions can be obtained from the correlation between projectile fragments and target-like fragments. For a large class of events we find no binary partners in the gas modules. We believe that a large fraction of these are not true binary fission events in which one fragment is not detected, but are the result of more violent collisions which leave a single hot residue in the fission mass range. The distribution of the largest Z seen in the forward hodoscope, $Z_{\max}^{\text{hodo}}$, in coincidence with two fission fragments detected in the gas modules is shown in Fig. 5(a). When a single fragment in the fission mass range is detected in the gas counters, the distribution of the coincident $Z_{\max}^{\text{hodo}}$ is bimodal as in Fig. 5(b). The peak at large Z values arises from peripheral collisions in which one of the fission fragments is not detected while the peak at low Z is due to hard collisions in which only a residue in the fission mass range remains. This behavior is consistent with previous results from Warwick *et al.* [10] who observed contributions from binary fission and "deep spallation" processes in the same mass interval for 200 MeV/nucleon Ne bombardments of Au.

The complete kinematic analysis of fission events can only be done if the charges and the velocities of both fragments are known. This restricts us to events where both laboratory velocities are between 1.0 and 2.3 cm/ns; outside this range we do not get Z information from the PC masks. The velocity distributions of the fission fragments in the laboratory frame have their most probable values at or below 1.5 cm/ns. Less than 1% of the fragments have velocities greater than 2.3 cm/ns indicating that we lose very little fission data due to this upper limit. The lower limit, on the other hand, excludes approximately one-half of the data, depending slightly on the target. However, because the relative velocity of the two

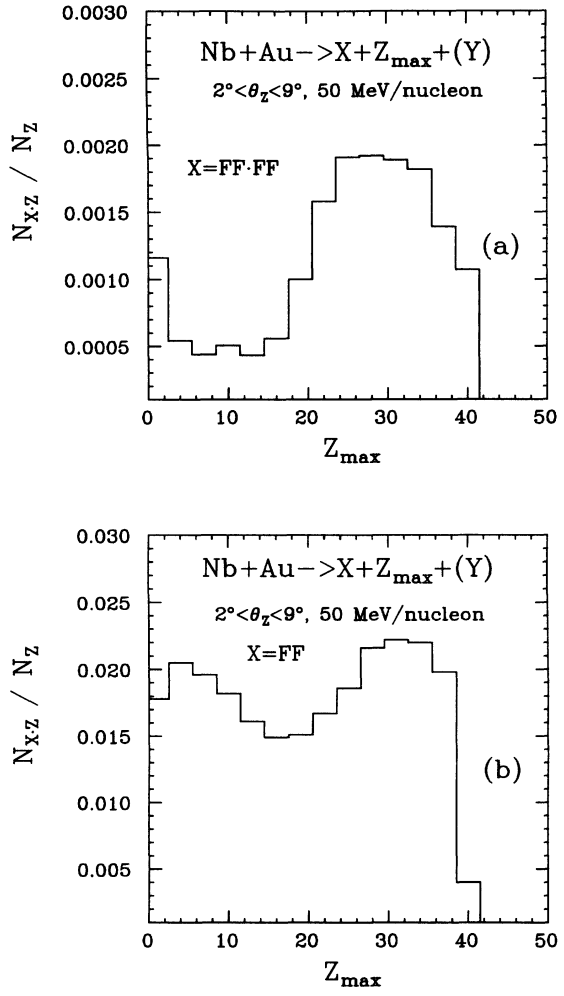

FIG. 5. (a) The ratio between coincidence and inclusive spectra of the largest fragment detected in the hodoscope for a coincidence with two fission mass fragments in the gas modules. (b) The same ratio except that now the coincidence is with only a single fission mass fragment.

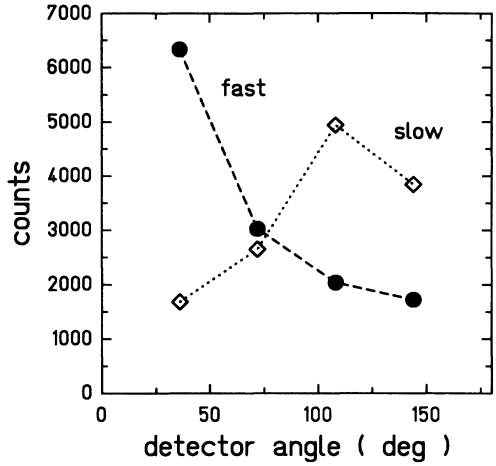

FIG. 6. Angular distribution of coincident fission fragments from 100 MeV/nucleon Nb+Au reactions detected on opposite sides of the beam with laboratory velocities less than (open symbols) and greater than (closed symbols) 1.0 cm/ns.

fragments is sharply peaked it is almost always true that when one fragment falls below this lower limit the other will be above it. In this case a clear fission identification is obtained. Fission fragments detected at backward angles are especially susceptible to the lower velocity limit. This is demonstrated in Fig. 6 which shows the angular distribution of fission fragments from binary coincidence events detected on different sides of the beam with laboratory velocities below and above 1.0 cm/ns for the system Nb+Au at 100 MeV/nucleon. The fast fragments are peaked forward whereas the slow fragments show an enhancement at backwards angles. To ascertain that this is indeed a purely kinematic effect, we compared the acceptance-corrected folding angle distributions for the two groups (two fast fragments versus one fast and one slow) and found that they are identical within experimental errors for all systems investigated. As an example, the distributions for the system Nb+Au at 100 MeV/nucleon are shown in Fig. 7. Therefore, we believe that the subset of data based on the coincidence of two fast fragments is a representative ensemble for all processes that lead to fission.

In order to extract the momenta from the experimentally determined quantities in events with two fast fragments, we must make an assumption concerning the relation between the charges of the detected fission fragments and the charge of the fissioning system. The deexcitation of the excited fission fragments is dominated by the evaporation of neutrons, so using $Z_{sum}=Z_1+Z_2$ as the charge of the fissioning system is a good approximation. The evaporation of neutrons does not change the mean values of the velocity distributions, but it does lower the mean values of the momenta.

The determination of the masses is more complicated.

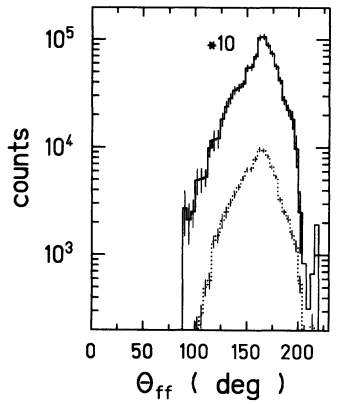

FIG. 7. Acceptance-corrected folding angle distributions for fission events from 100 MeV/nucleon Nb+Au reactions. The solid curve shows the distribution in which both fragments have velocities greater than 1.0 cm/ns (fast/fast); the dashed curve shows the distribution in which one of the fragments has a velocity less than 1.0 cm/ns (fast/slow). The shapes of the two distributions are identical.

Since the energy loss of a heavy particle in matter depends only on its charge and not on its mass, we have to make an assumption about the correlation between the atomic number and the mass of a detected particle. Two reasonable assumptions in the case of fission are that either the two fission fragments or the fissioning system itself are in the valley of stability. In both cases the masses can be estimated using the measured Z values. Due to the neutron excess in heavier nuclei the two possibilities give values for the momenta which are different by 10% to 15%. Since velocity is the primary quantity measured, this discrepancy can be avoided by calculating the momentum per nucleon instead of the total momentum, in which case both methods give to first order the same results. By using the momenta with the position information we can construct the complete kinematics of the fissioning source, i.e., calculate $P_{\parallel}$, $P_{\perp}$, and the pointing angle on an event-by-event basis.

III. RESULTS AND DISCUSSION

A. Mean values

Figure 8(a) shows the acceptance-corrected mean values of the $P_{\parallel}$ distributions for all the systems we have studied and for previous Ne+Au data at higher energies [10]. A comparison of the Nb+Au data with the Fe+Au data shows that the parallel momentum transferred to the target nucleus is essentially independent of the entrance channel. The decrease in mean $P_{\parallel}$ with increasing target mass is a result of the rapid increase in fissility from Ta to Th. In particular, fission of Ta requires relatively high excitation energies and/or angular momenta which are correlated with the largest $P_{\parallel}$ transfers. Further discussion and a comparison to predictions of a simple intranuclear cascade model with statistical decay of the target residue are presented in Ref. [2].

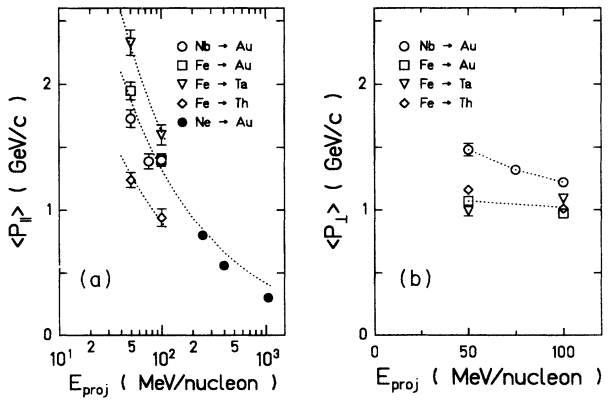

FIG. 8. (a) Average parallel and (b) average transverse momentum of the fissioning system as a function of projectile energy for the different systems investigated (open symbols). The solid symbols for the Ne+Au data are taken from Ref. [10]. The dotted curves in (a) show the dependence on the inverse square root of the projectile energy; the dotted curves in (b) are drawn to guide the eye.

For a given projectile/target combination the mean momentum transfer decreases with increasing beam energy. If fission occurs in a narrow range of excitation energies independent of the projectile energy and if the energy is deposited through the direct transfer of nucleons from the projectile to the target, then the most probable momentum transfer would decrease as the inverse of the square root of the beam energy. This simple dependence is shown by the dotted lines in Fig. 8(a). Our data exhibit such an energy dependence for all systems investigated. If the Au target results are extrapolated to higher energies we get a good fit to the previous Ne+Au measurements at 250–1050 MeV/nucleon [10,12].

Figure 8(b) shows the acceptance-corrected mean values for the $P_{\perp}$ versus the incident energy per nucleon. $P_{\perp}$ depends only on the projectile nucleus and on its energy, and shows a slight decrease with increasing energy. This trend can be reproduced by assuming that the momentum transfer is caused by the absorption of a few nucleons during a grazing collision. As Fig. 2(a) shows, the fission fragment acceptance for $P_{\perp}=2$ GeV/c is still approximately 25% of the maximum value. This means that the measurement of $P_{\perp}$ is not significantly restricted by limitations of our geometry.

Most previous experiments have utilized the fission fragment angular correlation technique [13] to estimate the parallel momentum transfer to the fissioning system. In this method the mean parallel momentum transfer is calculated from the mean folding angle. Systematics with a broad spectrum of energies and projectile masses have been obtained (see Ref. [1] for review). From these results, it is clear that fission at lower energies has large contributions from compoundlike processes while at higher energies peripheral reactions dominate. There is a broad transition in the 20–100 MeV/nucleon region depending on the mass of the projectile. For example, there is still a large compoundlike contribution for 25 MeV/nucleon Kr+Au but by 45 MeV/nucleon this contribution has completely disappeared and only peripheral fission remains [14]. Clearly our data for Fe and Nb projectiles are in the bombarding energy region where peripheral collisions dominate.

Based on limited previous data for $6 < A_{\rm proj} < 40$ it has been suggested [15] that there might be a universal relationship between $P_{\parallel}/A_{\rm proj}$ and $E/A_{\rm proj}$ which can describe the high energy heavy ion data for all projectiles. Conversely, the data could also be parametrized on the basis of a limiting average excitation energy of the fissioning nucleus. Saint-Laurent *et al.* [16] extracted from this parametrization a numerical value of 160 MeV for this average excitation energy in thorium nuclei. This number is based on the linear relation between fractional energy deposition and fractional momentum transfer [17]:

$$\frac{E^*}{E^*_{\rm CN}} = 0.75 \frac{p_{\parallel}}{p_{\parallel \rm CN}} , \tag{1}$$

where $E^*/E^*_{\rm CN}$ and $P_{\parallel}/P_{\parallel \rm CN}$ denote the excitation energy and the parallel momentum of the fissioning system

and the compound nucleus, respectively. The additional factor of 0.75 is not expected from the naive assumption that energy deposition and momentum transfer are caused by direct transfer of nucleons from the projectile to the target (see discussion of Fig. 8, above), but stems from INC calculations described in Ref. [17].

In our model calculations, presented in Ref. [2], it is shown that since fission is a slow process occurring near the end of the deexcitation cascade, only excitation energies up to a few hundred MeV produce a fissionable residue. At higher excitations, the equilibrated target residue becomes too light to fission. This trend may be accentuated by the onset of intermediate mass fragment emission which leads to even lighter target residues. However, our calculations yield a direct dependence of the fractional energy deposition on the fractional momentum transfer, i.e., without the additional factor of 0.75.

In Fig. 9 we present our Fe+Th data together with previous results. It is clear that our data are most consistent with the limiting energy concept, which leads to the $\sqrt{E_{\text{beam}}}$ energy dependence discussed above. Using our relation between the energy deposition and the momentum transfer we obtain a limiting average excitation energy of 220 MeV. The value is also in good agreement with the results for O and Ne projectiles at energies above 30 MeV/nucleon. Unfortunately no data exist for ions in the mass range between alpha particles and O for projectile energies above 50 MeV/nucleon, but above 200 MeV/nucleon even the results for alpha-induced fission are not inconsistent with the limiting energy concept.

There has been a lot of speculation about the parameters that limit fission in high energy nuclear reactions. Since fission is a complex process and the fission probability is affected by competing phenomena like preequilibrium emission, incomplete fusion, intermediate mass fragment production, and prefission nucleon evaporation, it is not *a priori* clear that data from a wide range of projectile masses and projectile energies follow a common systematics. But from the previous discussion we conclude that in the high energy region the most important parameter is the energy deposit into the nucleus. Our calculations indicate that one reaches the "natural end of fission" because nuclei with higher excitation energy deexcite via a fast cascade and finally end up with vanishing fission probability.

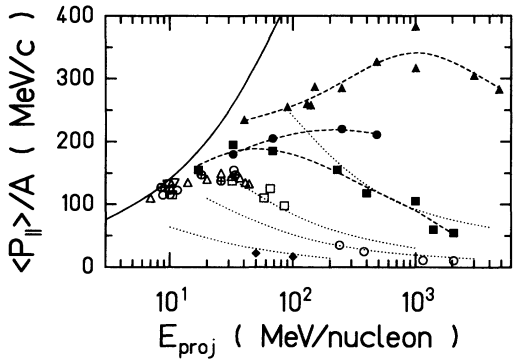

FIG. 9. Average parallel momentum per projectile nucleon as a function of projectile energy per nucleon for the fission of thorium and uranium by various projectiles. The solid triangles (protons), solid circles (deuterons), solid boxes (alphas) and open symbols (^{6}Li, ^{12}C, ^{14}N, ^{16}O, and ^{20}Ne) are data taken from Ref. [1]. Our Fe+Th fission data at 50 and 100 MeV/nucleon are included as the solid diamonds. The solid line indicates full momentum transfer while the dashed lines are drawn to guide the eye through the lighter projectile data. The dotted lines show the momentum transfer limitation due to the excitation energy limitation as discussed in the text and Ref. [16].

Figure 10 shows the distributions of the charge loss, $\Delta Z = Z_{\text{targ}} - Z_{\text{sum}}$, for all the systems investigated. Again the influence of the very different fissility parameters is obvious. Thorium fission is dominated by peripheral reactions with very low momentum transfer and little charge loss while a gold nucleus needs a higher momentum transfer to fission and we see the expected higher mean charge loss due to the deexcitation via particle evaporation. The ΔZ distributions for Nb+Au and Fe+Au are identical for both energies which means that the entrance channel does not determine the properties of the final fissioning systems as the parallel momentum distributions have already demonstrated. For tantalum, the mean values of the ΔZ distributions are shifted to still higher values indicating the high linear momentum transfer (excitation energy) necessary for fission. However, a high Z loss leaves a residual nucleus which is no longer highly fissile. Both effects together result in a ΔZ distribution which is less sharply peaked than the Au and Th distributions.

B. Total fission cross sections

We can calculate the total number of fission events from the folding angle distributions of all fission events (class I and class II) with the acceptance corrections described in Sec. II 3 (see Fig. 7). The resulting fission cross sections are presented in Table I and Fig. 11. The large error in the evaluation of the fission cross sections is

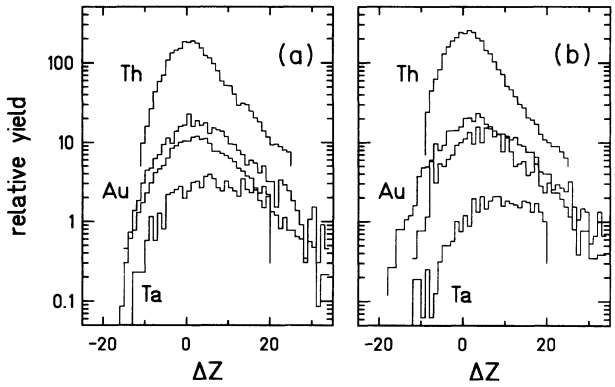

FIG. 10. (a) Fission charge loss distribution for Fe+Ta, Au, Th, and Nb+Au at 100 MeV/nucleon. (b) Fission charge loss distribution for the same systems but for a projectile energy of 50 MeV/nucleon. The gold data for the two projectiles are virtually identical; the upper gold curve in both panels is the Nb+Au reaction.

TABLE I. Fission cross sections.

Reaction	Beam energy (MeV/nucleon)	Fission cross section (mb)
Nb+Au	50	400±60
	75	271±60
	100	150±50
Fe+Ta	50	52±17
	100	32±11
Fe+Au	50	165±35
	100	165±40
Fe+Th	50	1810±250
	100	1930±470

mainly due to uncertainties in the integrated beam. We divided the estimated fission cross sections, σ_{fiss}, by the geometric cross sections, σ_{geo}, given by

$$\sigma_{\text{geo}}=\pi R_{\text{graz}}^2\left[1-\frac{V_{\text{Coul}}}{E_{\text{c.m.}}}\right] \tag{2}$$

with

$$R_{\text{graz}}=1.16(A_1^{1/3}+A_2^{1/3}+2)\ .$$

Here R_{graz} is the interaction radius, V_{Coul} the Coulomb repulsion, and $E_{\text{c.m.}}$ is the total center-of-mass energy. The data can then be compared to previous measurements with lighter projectiles. First we compare our thorium fission cross sections to the results of other experiments which used uranium and thorium targets and a wide variety of bombarding energies and projectiles with masses between 1 and 40. In Fig. 12(a) we show the fission probabilities versus the total energy of the projectiles [18–20]. It can be seen that the fission probability decreases with increasing energy almost independently of the size of the projectile from values near 100% for low projectile energies to approximately 20% at 10 GeV.

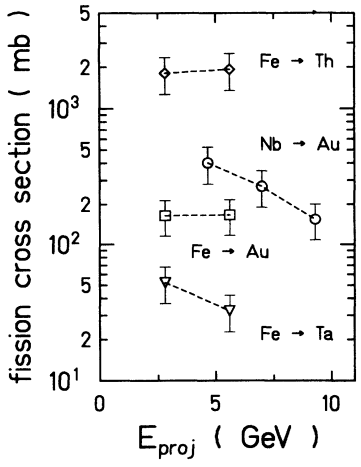

FIG. 11. Total fission cross sections for all systems investigated. The dashed lines are drawn to guide the eye.

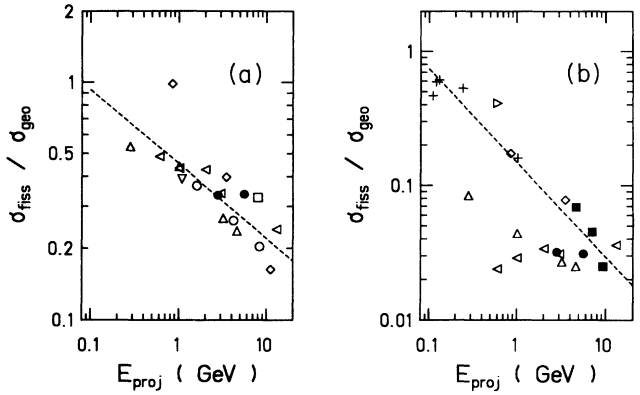

FIG. 12. (a) Fission excitation functions for thorium and uranium. (b) Fission excitation function for gold. The open symbols are taken from Refs. [18–24]; the solid circles and squares are our Fe and Nb induced fission data, respectively. The dashed lines are drawn to guide the eye.

In Fig. 12(b), we show the results for the Au target [19,21–24]. The trend is very similar to that for the fissile U and Th targets, but as the gold nucleus is not highly fissile, the angular momentum of the projectile in the entrance channel is an important quantity. The inherently low angular momentum transfers available in proton and alpha particle bombardments are qualitatively consistent with the low fission probabilities in these cases.

C. Relative fragment velocities

From our complete binary measurements we can construct the relative velocity ($|\mathbf{v}_1+\mathbf{v}_2|$) of the fission fragments in the rest frame of the fissioning system and then compare to known systematics for low energy fission [8]. It is of particular interest to look for possible higher fission velocities at the highest excitation energies (or ΔZ). Such effects have been reported for other systems [25,26] and could be a signal for a nonequilibrium fast fission process. In Fig. 13, we show the distribution of the relative velocities of binary events as function of ΔZ for the system Nb+Au at 100 MeV/nucleon. We find a narrow distribution centered at a value which is approximately 10% below the Viola velocity [8] for all events with $\Delta Z<30$. The deviation of these events from the Viola systematics can be completely attributed to energy loss in the target. For larger values of ΔZ, the mean value of the velocity starts to shift, and, more importantly, the distribution starts to broaden significantly, which is a clear indication that the reaction process for these events is not binary. This is also consistent with Fig. 4, where we showed the separation into a fission and a nonfission region in the Z_1-Z_2 plane. Collisions which lead to a total charge loss of more than 25 charge units clearly fall in the nonfission region.

For further evaluation of the data for consistency with the fission systematics, we also analyzed the folding angles as a function of the momentum transfer as derived

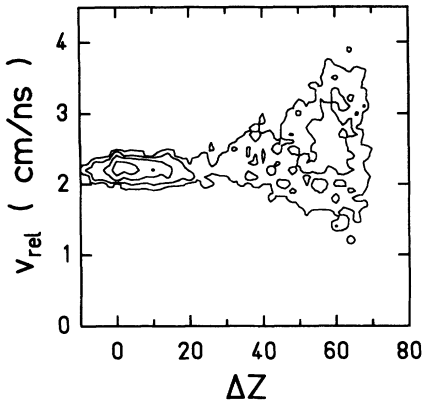

FIG. 13. Contour plot of the relative fragment velocity from binary events as a function of the charge loss for the reaction 100 MeV/nucleon Nb+Au. For values of ΔZ less than about 25, the velocities are tightly distributed around the Viola value [8]. For larger ΔZ, the distribution of velocities begins to broaden significantly. The contours represent an increase in yield by factors of 2.

from the velocity measurements. This provides a stringent test because the errors in the determination of the angles are significantly smaller than those for the velocities. The influence of a nonzero momentum of the fissioning nucleus is given by a velocity transformation in the laboratory frame and any deviation in the energy released during the fission process and, therefore, in the relative velocities of the fission fragments produces a corresponding deviation in the folding angle distribution. In Fig. 14, we plot the mean folding angle versus the parallel momentum transfer divided by A_f, where A_f is the estimated mass of the fissioning nucleus taking into account

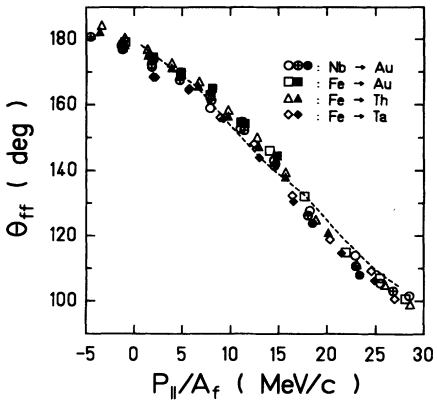

FIG. 14. Folding angles plotted as a function of $P_{\parallel}$ per nucleon of the fissioning system, A_f, for all systems studied in this work. The dashed curve is the result of a simulation based on Viola's [8] fission fragment velocity systematics and described in the text. The open symbols are the 100 MeV/nucleon projectile data and the closed symbols are the 50 MeV/nucleon projectile data; the single set of ⊗ points are the 75 MeV/nucleon Nb+Au data.

the mass loss ($\Delta A = A_{\text{targ}} - A_f$) before fission. The value for ΔA is estimated from the measured $\Delta Z = Z_{\text{targ}} - Z_f$, as discussed earlier. We compare the experimental distribution to a Monte Carlo simulation in which we take the detector geometry into account, assume Viola's velocity systematics [8], a symmetric Z distribution and isotropic emission in the rest frame of the fissioning system. For all systems the data fall on top of each other and within the experimental errors they agree with the simulations up to the highest values of momentum transfer. This means that in contradiction to Ref. [25] we observe no deviations from the low energy fission systematics [8] up to momentum transfers of 6 GeV/c, which is at least 10% of the total momentum in the reaction.

D. Systematics as a function of momentum transfer

Since we measure the momenta and charges for both fragments, it is possible with this data to study exclusive correlations that are not generally available from folding angle experiments. In particular, in our data the most interesting correlations are between parallel momentum transfer, perpendicular momentum transfer, and charge loss. We expect these to lead to further insight into the fission process and the limiting conditions for fission.

The distributions in $P_{\parallel}$ and $P_{\perp}$ for the systems studied are shown in Figs. 15 and 16. In the low energy tail of the $P_{\parallel}$ distribution, the sum of the parallel momenta of the two detected fragments may become negative due to particle evaporation during the deexcitation of the target residues. Therefore we also accumulated data for small negative $P_{\parallel}$.

First we discuss the behavior of the perpendicular

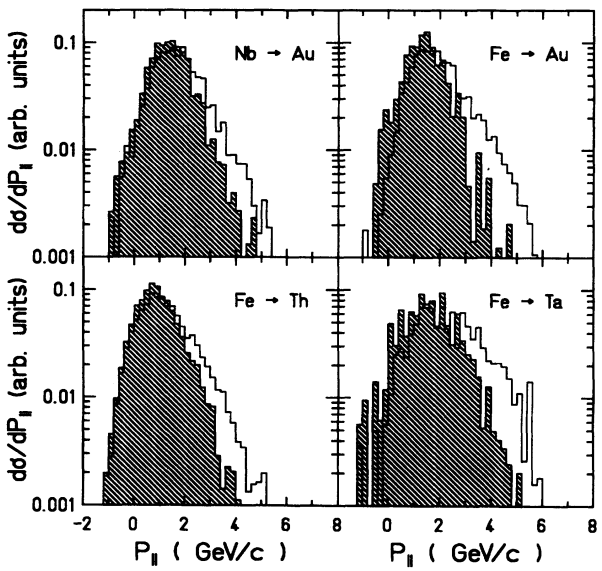

FIG. 15. Acceptance-corrected parallel momentum distributions for all systems investigated. The hatched and the open distributions show the 100 and 50 MeV/nucleon projectile data, respectively. The two spectra for a given system have been normalized to an equal number of counts to simplify the shape comparison.

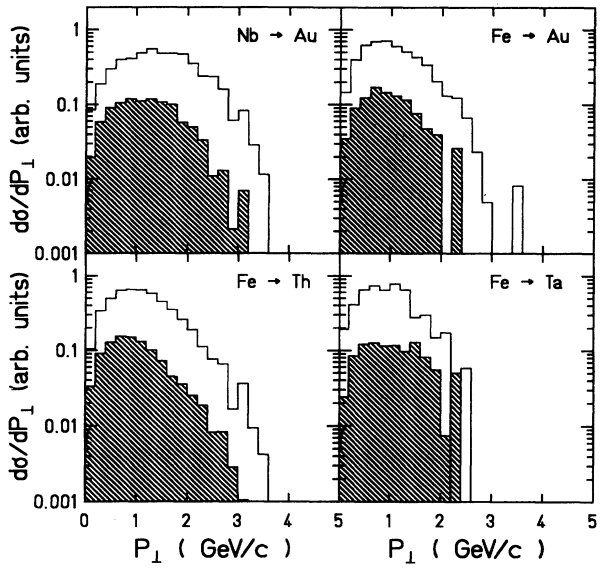

FIG. 16. Acceptance-corrected transverse momentum distributions for all systems investigated. The hatched and the open distributions show the 100 and 50 MeV/nucleon projectile data, respectively. As in Fig. 15, the two spectra for a given system have been normalized to an equal number of counts; however, the 50 MeV/nucleon spectra have been offset by an additional factor of 5.

momentum with increasing parallel momentum. Figure 17 shows that the perpendicular momenta of the fissioning nuclei are essentially independent of $P_{\parallel}$ for all systems and energies investigated. Like the mean values of $P_{\perp}$ shown earlier in Fig. 8, these distributions show a small decrease with increasing projectile energy and an increase with increasing projectile mass. The error bars show the variances of all the $P_{\perp}$ distributions and these widths also do not depend significantly on $P_{\parallel}$. These trends suggest that the transfer of perpendicular momentum is not strongly coupled to the transfer of parallel momentum. This result seems surprising at first since most models based on INC or incomplete fusion tend to predict that for the heavy residues left after the direct or preequilibrium reaction stage, the perpendicular and parallel components of the momentum transfer are roughly proportional. However, a detailed statistical calculation [2] which includes both INC and fission decay does reproduce the experimental results at 100 MeV/nucleon that are presented in this paper (see Ref. [2], Fig. 8).

Figure 18 shows the charge loss of the fissioning nucleus as a function of parallel momentum transfer. The results are approximately independent of projectile mass and energy. The difference in slope for different targets is consistent with the dependence expected due to the fissility differences between Ta, Au, and Th. The very simple correlation described below demonstrates the internal consistency of these results. The increase in ΔZ at low and negative $P_{\parallel}$ can be qualitatively understood as due to the tail of evaporation products originating near the peak of the $P_{\parallel}$ distributions for each target.

In order to look for possible projectile and target dependences we compare all of our data in a very simple parametrization that is similar to that used to interpret earlier ^{40}Ar data [27]. We assume that the linear momentum transfer can be attributed to the absorption of a few projectile nucleons by the target. The number of absorbed nucleons, m, can then be estimated using the linear momentum transfer to the fissioning system as

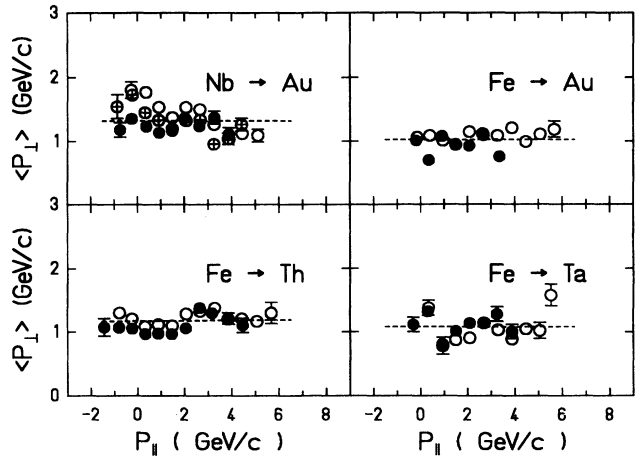

FIG. 17. Perpendicular vs parallel momentum transfer for all systems studied. The open and the solid symbols show the 50 and 100 MeV/nucleon projectile data, respectively. The ⊗ symbols in the upper left panel are the 75 MeV/nucleon Nb+Au data. The dashed lines are drawn to guide the eye.

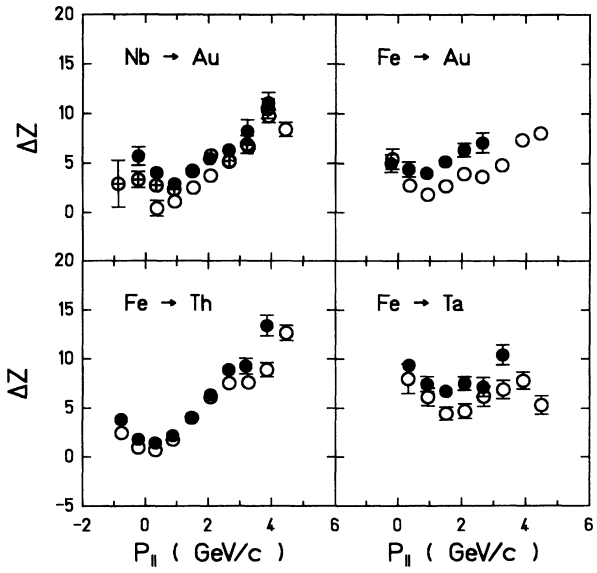

FIG. 18. Charge loss of the fission nucleus as a function of the parallel momentum transfer. The open and solid symbols show the 50 and 100 MeV/nucleon projectile data, respectively. The ⊗ symbols in the upper left panel are the 75 MeV/nucleon Nb+Au data.

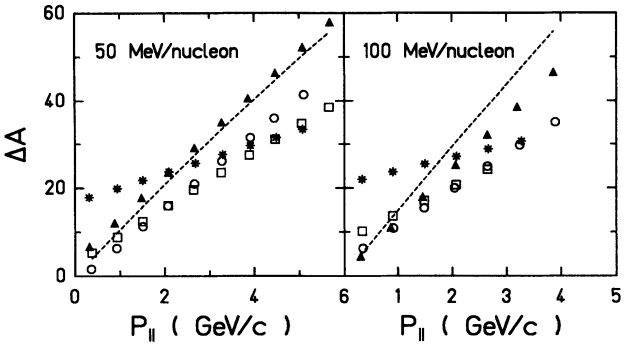

FIG. 19. The mass loss, ΔA, of the fissioning nucleus as a function of the parallel momentum transfer for all of the 50 and 100 MeV/nucleon projectile data. Stars: Fe+Ta; circles: Nb+Au; squares: Fe+Au; triangles: Fe+Th. The dashed lines are calculated using the model discussed in the text.

$$m = A_p \frac{P_\parallel}{P_i} , \tag{3}$$

where A_p is the mass of the projectile and P_i the incident linear momentum. The excitation energy, E^*, for this incomplete fusion process is then given by

$$E^* = E^*_{\rm CF} \frac{P_\parallel}{P_i} \frac{A_p + A_T}{m + A_T} , \tag{4}$$

where $E^*_{\rm CF}$ is the excitation energy for complete fusion. If we assume that the emission of a nucleon lowers the excitation energy on the average by 15 MeV, we can calculate the number of evaporated particles, $\Delta A^{\rm calc}$, for a given momentum transfer using

$$\Delta A^{\rm calc} = \frac{E^*}{15} . \tag{5}$$

On the other hand, we can also determine the number of emitted particles from the experimental data according to the relation

$$\Delta A^{\rm exp} = A_T + m - \overline{M}_T^{\rm exp} . \tag{6}$$

The mean mass observed for a given momentum transfer, $\overline{M}_T^{\rm exp}$, is calculated using the mean charge loss. The comparison of the $\Delta A^{\rm calc}$ and $\Delta A^{\rm exp}$ is shown in Fig. 19 for the projectile energies 50 and 100 MeV/nucleon. The agreement is remarkable for the Th and Au targets. The Ta data show deviations from the calculation which is not surprising. It should be emphasized that we are analyzing only fission events and that these are expected to be a representative subset of the whole data at a given momentum transfer only for systems with a reasonably high fissility. This is certainly the case for thorium and also to some extent for gold at not too high values of linear momentum transfer. Indeed we see deviations from the calculation in the case of gold for the largest momentum transfers due to the fact that high momentum transfer and subsequent high charge loss will lead to a system that is no longer highly fissile. In the case of tantalum, we can expect only the mean value for the mass loss corresponding to the mean parallel momentum of the inclusive momentum distribution to agree with the calculation, which is indeed the case.

IV. SUMMARY

In this paper we present results on the systematic behavior of fission from intermediate energy heavy ion reactions on heavy targets. The reactions studied are Nb+Au and Fe+Au, Ta, Th at beam energies of 50–100 MeV/nucleon. Inclusive and exclusive results are presented on the cross sections, parallel and perpendicular momentum transfer, and charge loss.

Detailed results are presented on the momentum transfer ($P_\parallel$ and $P_\perp$) and total charge of the fissioning system as well as the relative velocities of the fragments. The result agrees qualitatively with previous systematics with respect to both parallel momentum transfer and Z loss. A simple relation exists between the mass loss and parallel momentum transfer. This correlation is a result of the strong coupling of parallel momentum transfer to excitation energy. The apparent saturation of the perpendicular momentum transfer is reproduced in a detailed statistical treatment of these reactions presented in Ref. [2].

The results suggest a limiting excitation energy for reactions leading to fission in this energy regime. Such a limit can result from the lack of a target residue heavy enough to have an appreciable fission branch in cases where the initial target residue has an excitation energy above 1 GeV and emits many preequilibrium nucleons. This limit could alternatively result from the onset of multifragmentation processes. The present data are unable to distinguish the two possibilities. A more detailed model of these reactions in terms of a fast cascade followed by statistical decay is given in a companion paper [2].

The fission cross sections are consistent with previous systematics and show a decrease with increasing projectile energy. This behavior is also consistent with a limiting excitation energy for residues that subsequently fission.

ACKNOWLEDGMENTS

We are pleased to acknowledge the help of the LBL Bevalac staff in supporting these experiments. We would also like to acknowledge the hard work of Ron Marquardt (MIT) and James Larkin (Cal-State, Hayward). This work was performed under the auspices of the U.S. Department of Energy by the Lawrence Livermore National Laboratory under Contract W-7405-ENG-48, and by contracts with the Department of Energy with Los Alamos National Laboratory under Contract W-7405-ENG-36, Lawrence Berkeley Laboratory under Contract DE-AC03-76SF00098 and Argonne National Laboratory under Contract W-31-109-ENG-38.

[1] V. E. Viola, Nucl. Phys. **A502**, 531c (1989).
[2] Th. Blaich, M. Begemann-Blaich, M. M. Fowler, J. B. Wilhelmy, H. C. Britt, D. J. Fields, L. F. Hansen, M. N. Namboodiri, T. C. Sangster, and Z. Fraenkel, Phys. Rev. C **45**, 689 (1992), the following paper.
[3] M. M. Fowler *et al.*, Nucl. Instrum. Methods, **A281**, 527 (1989).
[4] Code based on K. Braune, D. Schwalm, GSI Jahresbericht, 1976.
[5] W. G. Meyer (private communication). The code is based on the Bethe formula.
[6] Code based on J. F. Ziegler, J. P. Biersack, and U. Littmark, *The Stopping and the Range of Ions in Solids* (Pergamon, New York, 1985).
[7] H. W. Schmitt, J. H. Neiler, and F. J. Walter, Phys. Rev. **141**, 1146 (1966).
[8] V. E. Viola, Nucl. Data, Sect. A **1**, 391 (1966); V. E. Viola, K. Kwiatkowski and M. Walker, Phys. Rev. C **31**, 1550 (1983).
[9] M. N. Namboodiri *et al.*, *Nuclear Dynamics and Nuclear Disassembly,* edited by J. Natowitz (World Scientific, Singapore, 1990); D. J. Fields *et al.*, Nucl. Phys. **A495**, 209c (1989).
[10] A. Warwick, H. H. Wieman, H. H. Gutbrod, M. R. Maier, J. Peter, H. G. Ritter, H. Stelzer, and F. Weik, Phys. Rev. C **27**, 1083 (1983).
[11] G. Klotz-Engmann, H. Oeschler, and E. Kankeleit, Phys. Lett. B **187**, 245 (1987).
[12] S. Kaufman *et al.*, Phys. Rev. C **26**, 2694 (1982).
[13] T. Sikkeland, E. L. Haines, and V. E. Viola, Phys. Rev. **125**, 1350 (1962).
[14] E. C. Pollacco, Y. Cassagnou, M. Conjeaud, R. Dayras, S. Harar, R. Legrain, J. E. Sauvestre, and C. Volant, Nucl. Phys. **A488**, 319c (1988).
[15] M. Fatyga, K. Kwiatkowski, H. J. Karwowski, L. W. Woo, and V. E. Viola, Phys. Rev. C **32**, 1496 (1985).
[16] F. Saint-Laurent, M. Conjeaud, R. Dayras, S. Harar, H. Oeschler, and C. Volant, Phys. Lett. **110B**, 372 (1982); F. Saint Laurent, M. Conjeaud, R. Dayras, S. Harar, H. Oeschler, and C. Volant, Nucl. Phys. **A422**, 307 (1984).
[17] N. T. Porile, Phys. Rev. **120**, 572 (1960).
[18] W. G. Meyer and H. H. Gutbrod, Phys. Rev. C **22**, 179 (1980).
[19] S. Harar, Nucl. Phys. **A471**, 205c (1987).
[20] D. Jacquet, E. Duek, J. M. Alexander, B. Borderie, J. Galin, D. Gardes, D. Guerreau, M. Lefort, F. Monnet, M. F. Rivet, and X. Tarrago, Phys. Rev. Lett. **53**, 2226 (1984).
[21] J. Hudis and S. Katcoff, Phys. Rev. C **13**, 1961 (1976).
[22] G. La Rana *et al.*, Nucl. Phys. **A407**, 233 (1983).
[23] H. Kudo, K. I. Moody, and G. T. Seaborg, Phys. Rev. C **30**, 1561 (1984).
[24] U. Lynen *et al.*, Nucl. Phys. **A387**, 129c (1982).
[25] M. Mostefai, Y. Cassagnou, M. Conjeaud, R. Dayras, S. Harar, R. Legrain, E. C. Pollaco, C. Volant, G. Klotz-Engmann, and H. Oeschler, J. Phys. (Paris) **C4**-47, 361 (1986).
[26] B. D. Wilkins, S. B. Kaufman, E. P. Steinberg, J. A. Urbon, and D. J. Henderson, Phys. Rev. Lett. **43**, 1080 (1979).
[27] Y. Cassagnou *et al.*, J. Phys. Soc. Jpn., Suppl. **54-2**, 422 (1985).